Study of the Effects of ECH Power and Pulse Length on Preionization in the KSTAR Tokamak

Young-soon Bae, Won Namkung, *Member, IEEE*, Moo Hyun Cho, and Alan C. England

***Abstract*—In this paper, we present the results of a study of the preionization effects for the Korean Superconducting Tokamak Advanced Research (KSTAR) tokamak ($R_0 = 1.8$ m, $a = 0.5$ m, $\kappa = 2, \delta = 0.8, B_T = 3.5$ T, $I_p = 2$ MA, $T_{\rm pulse} = 300$ s) that is under construction by the Korea Basic Science Institute (KBSI). The preionization will be given by the Electron Cyclotron Heating (ECH) System with an 84-GHz 500-kW gyrotron tube being made by Communications and Power Industries. The ECH preionization effects are investigated by a 0-dimensional code (TECHP0D[1]) that includes the operational scenarios of KSTAR tokamak. The code is now improved and advanced with carbon, oxygen, and iron impurity effects, and with the self and mutual inductances of seven pairs of superconducting poloidal coils for the KSTAR tokamak.**

***Index Terms*—Electron cyclotron heating (ECH), gyrotron, Korean superconducting tokamak advanced research (KSTAR), poloidal, preionization.**

I. Introduction

ELECTRON cyclotron heating (ECH) preionization has been successfully applied in a variety of tokamaks and is normally used to produce the plasma in contemporary stellarators. The general conclusion of these experiments is that ECH was effective in producing a good plasma which would: (a) reduce the startup runaway electrons; (b) reduce the voltage required to start the plasma current; and (c) somewhat reduce the Volt-s expenditure from the transformer needed to establish the plasma. The motivation for many of those experiments was the pioneering work of Peng *et al.* [1]. While some of the predictions of the theory were not born out by the experiments, nevertheless, the theory was important in showing the value of preionization for voltage reduction. On the basis of the experimental work by Kulchar *et al.* [2], a model was produced which was able to adequately describe the experiments in ISX-B. Later experimental work included the large tokamak experiments in T-10 [3] and DIII-D [4]. The Modeling efforts of Fidone and Granata [5] showed that for a large tokamak, energy deposition would not occur at the electron cyclotron resonance heating (ECRH) layer. Maroli and Petrillo [6] added plasma radial growth and impurities. Lloyd *et al.* [7] produced a more advanced model and added the effect of impurities, but did not consider the error field effects and poloidal field coil circuit equations.

Because of the thick vacuum vessel wall, superconducting poloidal field coils, and the concomitant limited current ramp rates, the generated loop voltage for breakdown may be too low to provide breakdown reliably in the Korean superconducting advanced research (KSTAR) tokamak [8]. As will be shown in the following, the current buildup time is more than 1 s. Eventually, the plasma duration will be 300 s. For KSTAR tokamak, preionization was studied earlier using the 0-dimensional (0-D) code (TECHP0D) for many other initial conditions [9]–[11] considering the effects of the error field and impurities. However, KSTAR has seven pairs of superconducting poloidal field coils that are controlled independently, we made a more advanced code to which the additional circuit parameter are added with circuit parameters of self inductances and mutual inductances. These parameters were calculated by KBSI [12]. Therefore, in the present set of calculations, the effect of the additional circuit equations is examined.

This paper presents subsequent results of the preionization simulation using this advanced code that is quite adequate for describing the physical process in KSTAR tokamak of major radius $R_0 = 1.8$ m and minor radius $a = 0.5$ m. The code is 0-D so that the elongation κ and triangularity δ are not relevant parameters. Similarly, the effect of variation of the initial minor radius a is not examined. The present version of the code allows the minor radius to grow but the radius is held constant for these studies. The variation of the minor radius would introduce an artificiality into the results that is not justified by the 0-D character of the code. Similarly, whether the energy deposition is at the ECR layer or the upper hybrid layer is not relevant to the results. The complexity of the plasma expanding in minor radius can be the subject of future studies. Previously, it has also been found [2] that the best results are obtained with a parallel index of refraction, $n_{||}$ of 0.5 and 100% X-mode polarization. This implies that the radiation incident on the plasma either from the high-field side or from the low-field side is transformed by a polarization rotator on the inside wall and reflected back to the plasma as X-mode.

II. Preionization Model

The model of the preionization was first applied to the ISX-B tokamak for early preionization experiments [2], [13]. As we already mentioned, more advanced models have appeared since that time [5]–[7]. The model in use here includes the circuit equations of seven pairs of controlled PF coils and the effects of hydrogen ions and impurities. Except for the impurity effects

Manuscript received October 28, 2002; revised May 5, 2003. This work was supported by the Korea Basic Science Institute (KBSI) and by the Korea Atomic Energy Research Institute (KAERI).

Y. S. Bae, W. Namkung, and M. H. Cho are with the Pohang University of Science and Technology, Pohang 790-784, Korea (e-mail: ysbae7@postech.ac.kr).

A. C. England is with the Korea Basic Science Institute, Daejon 305-333, Korea.

Digital Object Identifier 10.1109/TPS.2003.815474

[1]0-Dimensional Tokamak ECH Preionization code.

0093-3813/03$17.00 © 2003 IEEE

and the additional circuit equations for the KSTAR tokamak, a detailed discussion of the other equations is found in the previous paper [2]. The five main equations are as follows: 1) the continuity equation; 2) the density conservation equation, i.e., the time variation of the neutral density is the same as that of the electron density; 3) the electron energy density equation; 4) the ion energy density equation; and 5) the circuit equation. Here, we describe the circuit equation for the KSTAR tokamak, the energy density equations, and the radiation power due to impurities. Inclusion of hydrogen ions and impurities gives the time variations of the energy densities as shown in the following:

$$\frac{dU_e}{dt} = \frac{P_{\rm ECH} + P_{\rm OH} - P_{\rm IONIZ}}{V} - U_e(\nu_{\rm err} + \nu_{\rm dr} + \nu_E) - \frac{1}{V}(P_{\rm EQU} + P_{\rm BREM} + P_{\rm IRAD}) \quad (1)$$

$$\frac{dU_i}{dt} = \frac{1}{V}(P_{\rm EQU} - P_{\rm CX}) - U_i\nu_E \quad (2)$$

where V is the plasma volume $(2\pi R_0 \pi a^2), U_e$ is the electron energy density, and U_i is the ion energy density. $P_{\rm ECH}$ is the ECH power coupled to the plasma given as $P_{\rm ECH} = P_{\rm RF}[1 - f_o \exp(-\eta_o) - f_x \exp(-\eta_x)]$ [14], where $P_{\rm RF}$ is the RF power delivered to the plasma, η_o and η_x are the dimensionless optical depths for the ordinary mode and extraordinary mode, and f_o and f_x are the fractional powers for the ordinary and extraordinary modes, respectively. $P_{\rm OH}$ is the ohmic heating power given as simply $I_p^2 R_p$, where I_p is the plasma current and R_p is the plasma resistance. $P_{\rm IONIZ}$ is the ionization and radiation loss due to ionization and the radiation emitted by the energy level change processes, $P_{\rm EQU}$ is the power transferred from electrons to ions by equipartition, $P_{\rm BREM}$ is the bremsstrahlung power loss due to the hydrogen and impurity ions, and $P_{\rm CX}$ is the charge exchange power loss between hydrogen atom and hydrogen ions. The detail formulas of $P_{\rm IONIZ}, P_{\rm EQU}, P_{\rm BREM}$, and $P_{\rm CX}$ are described in [7]. $P_{\rm IRAD}$ is the fraction of the power lost from the line radiation through the interaction between electrons and impurities [15]. All of the power expressions have analytic forms except for the impurity line radiation power loss ($P_{\rm IRAD}$) expressions that are obtained from fittings to the experimental data. The fitted formulas of $P_{\rm IRAD}$ are made from the Figs. 3(f), 4(f), and 5(f) of [15] for the carbon, oxygen, and iron impurities, respectively. Carbon, oxygen, and iron are chosen because they are the most probable impurities due to the expected composition of the first wall (special carbon composite on the stainless-steel vessel). The fitted formulas are of the form

$$P_{\rm IRAD} = 10^6 \times N_e N_I \times 10^f \ [{\rm W/cm^3}] \quad (3)$$

where, $f = -33.93 + 4.888Q - 2.432Q^2 + 0.3697Q^3$ for the carbon impurity, $f = -34.06 + 4.194Q - 1.827Q^2 + 0.2467Q^3$ for the oxygen impurity, and $f = -30.23 - 0.152Q + 0.073Q^2 - 0.020Q^3$ for the iron impurity with $Q = \log(T_e)$. For these fittings, the curve labeled $10^{14} n_e \tau_i$ is chosen to see the distinguishable impurity effects. The impurity ion density is assumed to be produced with a variable influx rate, i.e., $N_I = F_I N_e$, where F_I is the fraction of the impurity to the electron density. It is easily understood that the variable influx rate gives the constant N_I/N_H considering $N_H = N_e - \sum_I Z_I N_I$ where N_H is the hydrogen ion density and Z_I is the atomic number of the impurity. The error field loss rate $\nu_{\rm err}$ is given as

$$\nu_{\rm err} = \left(\frac{\delta B}{B}\right)\left(\frac{V_T}{a}\right)\left[1 - \left(\frac{I_p}{I_c}\right)\right], \quad \text{for } I_p < I_c$$
$$= 0, \quad \text{for } I_p \geq I_c, \quad (4)$$

where, V_T is the electron thermal velocity, a is the minor radius of the plasma, and I_c is the critical current, $I_c = 4\pi a \delta B/\mu_0$. The larger anticipated field errors may mean that there is no poloidal field null in the vacuum vessel. The ν_{dr} is the drift loss rate [16], and the energy loss rate ν_E is given by the empirical law from "Alcator scaling" [17] when the plasma current is greater than the critical current. When the plasma current is lower than the critical current, the energy loss rate is scaled by the ratio of the plasma current to the critical current. Both electrons and ions loss rates are assumed to obey Alcator scaling since the temperatures are low.

TABLE I
SELF AND MUTUAL INDUCTANCES BETWEEN SEVEN PAIRS OF POLOIDAL FIELD COILS AND PLASMA IN UNITS OF mH

	PF1	PF2	PF3	PF4	PF5	PF6	PF7	Plasma
PF1	85.6	26.55	5.96	5.28	7.45	7.13	8.3	0.11
PF2	26.55	44.98	12.56	9.18	7.85	5.81	6.47	0.073
PF3	5.96	12.56	13.43	10.38	5.3	2.96	3.13	0.037
PF4	5.29	9.18	10.38	26.93	10.96	4.48	4.52	0.031
PF5	7.45	7.85	5.3	10.96	327.4	37.32	31.21	0.135
PF6	7.13	5.81	2.95	4.48	37.31	199.36	99.1	0.219
PF7	8.3	6.47	3.13	4.52	31.2	99.1	316.45	0.284
Plasma	0.11	0.073	0.037	0.031	0.135	0.219	0.284	0.003

The circuit equation for the seven pairs of the KSTAR PF coils is

$$-\sum_{n=1}^{8} M_{n8}\frac{dI_n}{dt} - I_8 R_p = 0. \quad (5)$$

In (5), $n = 1 - 7$ are indexes for the seven pairs of PF coils and $n = 8$ is for the plasma, R_p is the plasma resistance, and M_{n8} are the mutual inductances between the PF coils and the plasma. From (5), we get the plasma current change over dt

$$dI_8 = \frac{-\sum_{n=1}^{7} M_{n8}\frac{dI_n}{dt} - I_8 R_p}{M_{88}} dt. \quad (6)$$

The data for the mutual inductances between the PF coils and the plasma and for the self inductance of the plasma are calculated and listed in Table I. The rate of change of the currents in the PF coils dI_n/dt are assumed to be given by constant values between the specified times as specified for the first phase of the KSTAR tokamak operation [18]. Equation (6) is the difference between the externally applied loop voltage and the resistive voltage of the plasma. The externally applied loop voltage is

$$V_L = -\sum_{n=1}^{7} M_{n8}\frac{dI_n}{dt} \quad (7)$$

and the resistive voltage is

$$V_R = I_8 R_p. \quad (8)$$

The plasma resistance is

$$R_p = \frac{2\pi R_0}{\pi a^2}\frac{1}{2\sigma_\perp}. \tag{9}$$

The plasma conductivity $\sigma_\perp$ is given as follows:

$$\sigma_\perp = \frac{\omega_p^2}{4\pi(\nu_{\rm ei}+\nu_{\rm eo})}. \tag{10}$$

The electron–ion collision rate $\nu_{\rm ei}$ and the electron–atom collision rate $\nu_{\rm eo}$ are found in the NRL formulary [19].

III. Results

There are three kinds of input conditions—one for the microwave source, another for the KSTAR plasma, and the other for the poloidal field (PF) coils. The microwave source for the KSTAR ECH system is a CPI gyrotron tube. The gyrotron tube can generate a maximum of 500 kW with pulse lengths up to 2.0 s. However, the power delivered to the plasma through the waveguide and mirror-optics system is smaller than 500 kW due to various effects such as mode conversion, resistive losses, optical losses, etc. From the KSTAR ECH system design, the total power lost is 9%, so that the delivered power to the KSTAR plasma is approximately 455 kW. Since the power and the pulse length can be adjusted by the gyrotron power supply, the power and the pulse length are employed as the input parameter in the simulation. For the KSTAR plasma, we consider the following input parameters: the major radius ($R_0 = 1.8$ m), the minor radius ($a = 0.5$ m), the initial neutral density (N_0), the error field ($B_{\rm err}$), and the impurities such as carbon, oxygen, and iron. The major radius and minor radius are fixed in all simulations. The condition for the PF coils is already explained in the previous section. The important parameter for the PF coils is the beginning time ($T_{\rm OH}$) of the current sweep of the coils after the ECH power is turned on at time $\mathrm{T} = 0$. We call $T_{\rm OH}$ as the ohmic heating delay time.

A. Temporal Behaviors of Plasma Parameters

The following initial conditions are used: $P_{\rm RF} = 455$ kW for duration of 2.0 s, $T_{\rm OH} = 100$ ms, $R_0 = 1.8$ m, $a = 0.5$ m, $N_0 = 1.0 \times 10^{19}$ m^{-3}, $B_{\rm err} = 2.0$ mT. Fig. 1 shows the temporal behaviors of the electron temperature (T_e), the plasma current (I_p), the loop voltage (V_L), the resistive voltage (V_R), the electron density (N_e), the electron energy density (U_e), and the PF coil currents ($I_{\rm PFs}$) without considering any impurities. Fig. 2 shows the impurity effects on the output parameters for the carbon density of 0.001 N_e, oxygen density of 0.001 N_e, and iron density of 6.8×10^{-5} N_e. The impurities delay the time when the electron temperature starts to increase before the ohmic heating turn-on time. The impurities also cause the plasma to reach lower maximum electron temperature and plasma current. These figures show that when an RF power of 455 kW with a duration of 2.0 s is applied, the maximum T_e and I_p is reached before 1.5 s. The PF coil currents are designed to begin a plasma current ramp down at ~1.4 s after the time $T_{\rm OH}$. Hence, the preionization after the time of 1.4 s plus $T_{\rm OH}$ is unnecessary. Therefore, the upper limit of the calculation time is set to 1.5 s in subsequent calculations with $T_{\rm OH} = 100$ ms, and which is sufficient for finding the maximum electron temperature and the maximum plasma current.

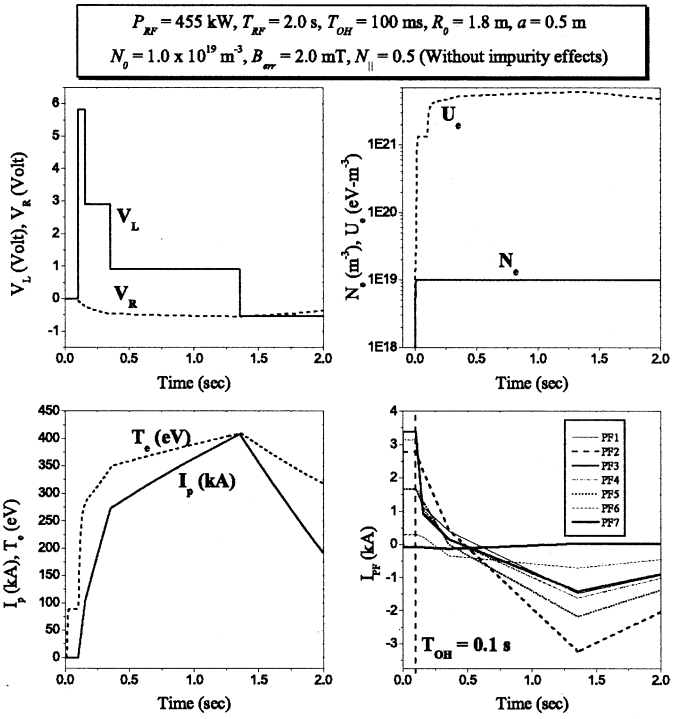

Fig. 1. Temporal behaviors of plasma parameters with initial conditions: $P_{\rm RF} = 455$ kW for duration of 2.0 s; $T_{\rm OH} = 100$ ms; $R_0 = 1.8$ m; $a = 0.5$ m; $N_0 = 1.0 \times 10^{19}$ m^{-3}; $B_{\rm err} = 2.0$ mT; and no impurities.

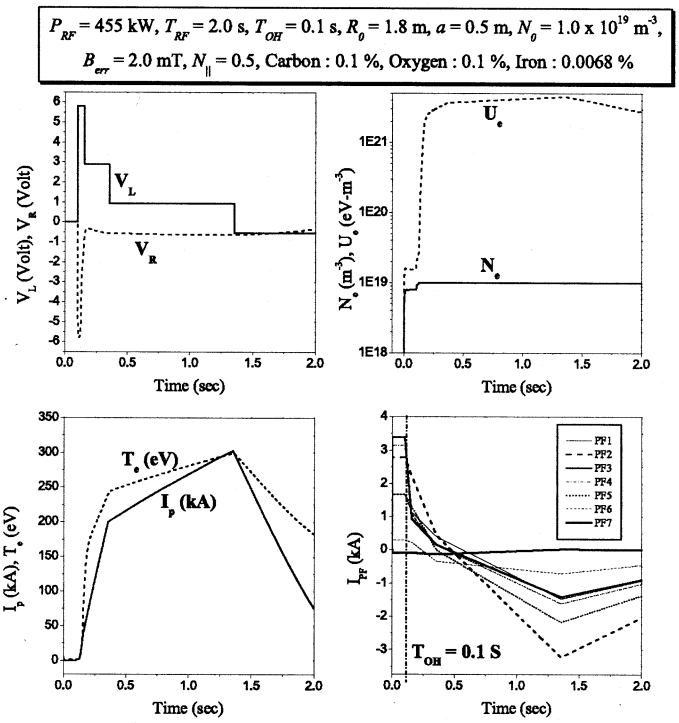

Fig. 2. Temporal behaviors of plasma parameters with initial conditions: $P_{\rm RF} = 455$ kW for duration of 2.0 s; $T_{\rm OH} = 100$ ms; $R_0 = 1.8$ m; $a = 0.5$ m; $N_0 = 1.0 \times 10^{19}$ m^{-3}, $B_{\rm err} = 2.0$ mT; carbon density $= 0.001\ N_e$, oxygen density $= 0.001\ N_e$; and iron density $= 6.8 \times 10^{-5}\ N_e$.

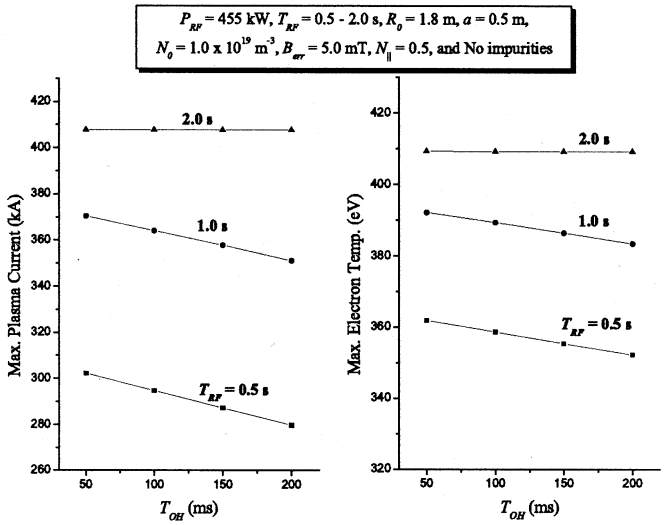

Fig. 3. Maximum plasma current and electron temperature as a function of the ohmic heating delay time ($T_{\rm OH}$) for an RF power $P_{\rm RF} = 455$ kW with durations of 0.5, 1.0, and 2.0 s.

B. Ohmic Heating Delay Time ($T_{\rm OH}$) Effects

The following initial conditions are used: RF power $P_{\rm RF} = 455$ kW with durations of 0.5, 1.0, 2.0 s, initial neutral density $N_0 = 1.0 \times 10^{19}$ m^{-3}, error field $B_{\rm err} = 5.0$ mT, and ohmic heating delay time $T_{\rm OH}$ varied between 50 and 200 ms. The maximum T_e and I_p are shown in Fig. 3. The maximum electron temperature and the maximum plasma current decrease as the ohmic heating delay time increases except for the case of 2.0-s ECH duration. For a 2-s pulse length, the maximum T_e and I_p do not depend on the $T_{\rm OH}$ since the ramp-down of the coil current starts at 1.4 s after the beginning of the ramp-up. If the $T_{\rm OH}$ was scanned longer than 600 ms, the maximum T_e and I_p would decrease even in the case of RF pulse duration of 2 s.

C. Initial Neutral Density (N_0) Effects

The following initial conditions are used: initial neutral density N_0 varied between 0.2×10^{19} m^{-3} and 1.2×10^{19} m^{-3}; error field $B_{\rm err} = 5.0$ mT; and ohmic heating delay time $T_{\rm OH} = 100$ ms (1) for $P_{\rm RF} = 455$ kW with durations of 0.5, 1.0, 1.5 s, (2) and $P_{\rm RF} = 100$ kW–500 kW with a duration of 1.5 s. Figs. 4 and 5 show the maximum T_e and maximum I_p. As the pulse length and the power increase, it is observed that the maximum plasma current and electron temperature increase and the dependence of I_p and T_e on the initial neutral density becomes small. The maximum plasma current increases slightly but the maximum electron temperature decreases as the initial neutral density increases. In the case of different powers with a pulse length of 1.5 s (Fig. 5), there exists a threshold power for a given initial neutral density. The threshold power is 200 kW for $N_0 = 1.0 \times 10^{19}$ m^{-3}. Fig. 5 shows that it is required to have a higher threshold power as the initial neutral density increases.

D. Error Field ($B_{\rm err}$) Effects

The following initial conditions are used: initial neutral density $N_0 = 1.0 \times 10^{19}$ m^{-3}; error field $B_{\rm err}$ varied between 1.0 and 5.0 mT; and ohmic heating delay time $T_{\rm OH} = 100$ ms (1) for $P_{\rm RF} = 455$ kW with durations of 0.5, 1.0, 1.5 s; (2) and for $P_{\rm RF} = 100$ kW–500 kW with a duration of 1.5 s. Figs. 6 and 7 show the maximum T_e and maximum I_p. Similar to the initial neutral density effects, it is seen that the maximum plasma current and electron temperature increase as the pulse length and the power increase. However, for an RF power more than 300 kW, the error fields do not influence the plasma current and electron temperature as shown in Figs. 6 and 7. In this case, there also exists a threshold power for the error field of 4 mT. Fig. 7 shows that if more than 200 kW power is applied for a duration of 1.5 s, the plasma current and the electron temperature are rather slowly varying.

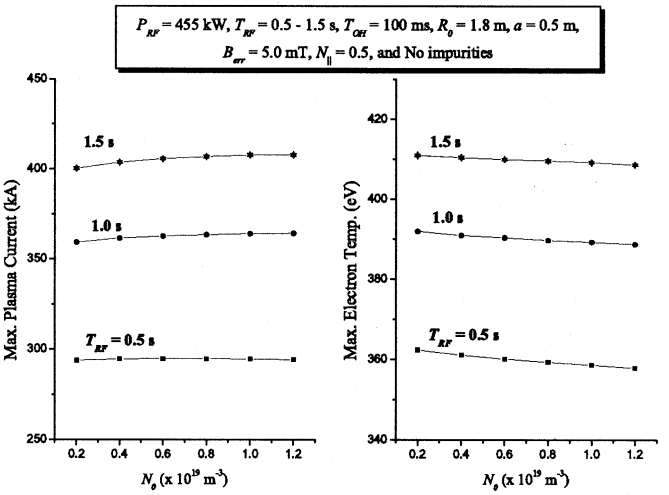

Fig. 4. Maximum plasma current and electron temperature as a function of the initial neutral density (N_0) for an RF power $P_{\rm RF} = 455$ kW with durations of 0.5, 1.0, and 1.5 s.

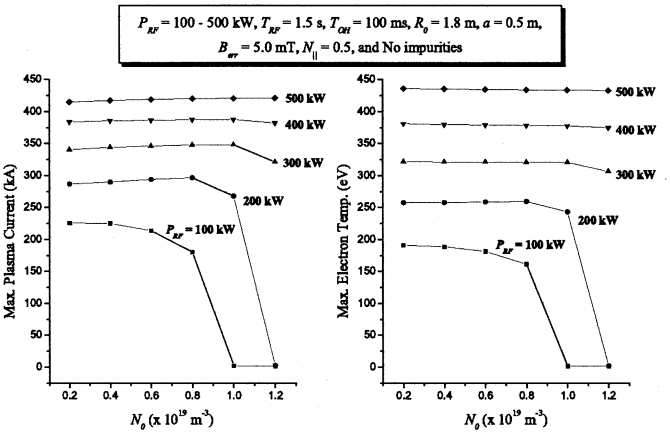

Fig. 5. Maximum plasma current and electron temperature as a function of the initial neutral density (N_0) for RF powers of $P_{\rm RF} = 100$ kW–500 kW with a duration of 1.5 s.

E. Impurities Effects

We consider carbon, oxygen, and iron impurities. There are little differences between the carbon and oxygen impurity effects. However, the iron impurity effect is larger than that of carbon and oxygen. To calculate these effects, the following initial conditions are used: initial neutral density $N_0 = 1.0 \times 10^{19}$ m^{-3}; error field $B_{\rm err} = 5.0$ mT;, and ohmic heating delay

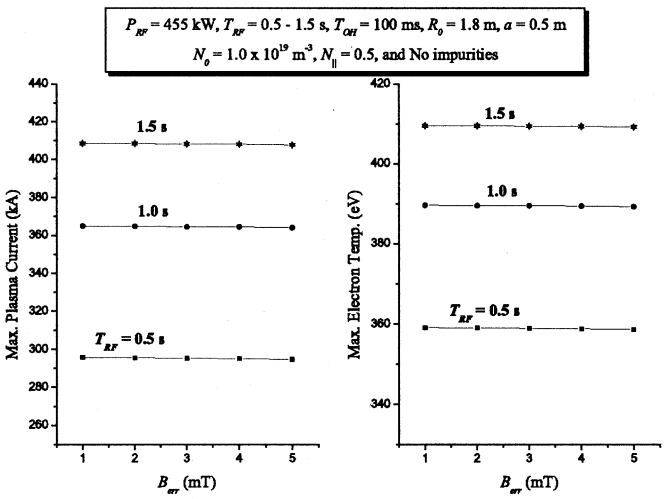

Fig. 6. Maximum plasma current and electron temperature as a function of the error field (B_{err}) for an RF power $P_{\mathrm{RF}} = 455$ kW with durations of 0.5, 1.0, and 1.5 s.

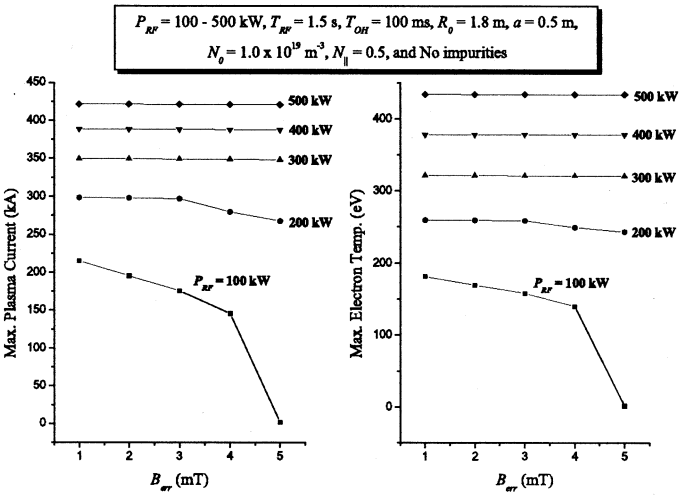

Fig. 7. Maximum plasma current and electron temperature as a function of the error field (B_{err}) for RF powers of $P_{\mathrm{RF}} = 100$ kW–500 kW with a duration of 1.5 s.

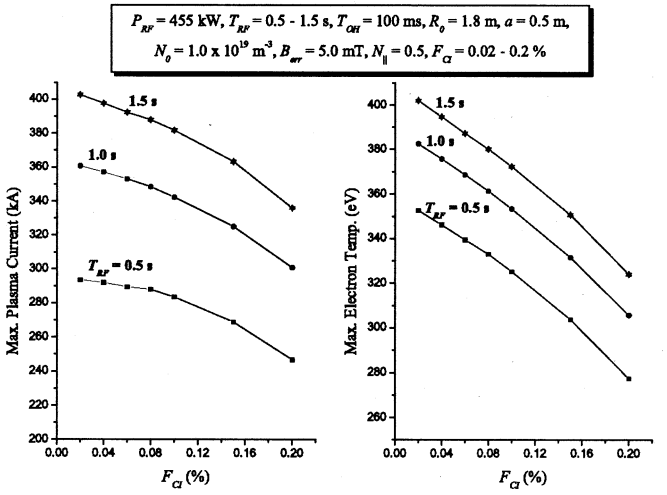

Fig. 8. Maximum plasma current and electron temperature as a function of the fraction of the carbon impurity (F_{CI}) to the electron density for an RF power $P_{\mathrm{RF}} = 455$ kW with durations of 0.5, 1.0, and 1.5 s.

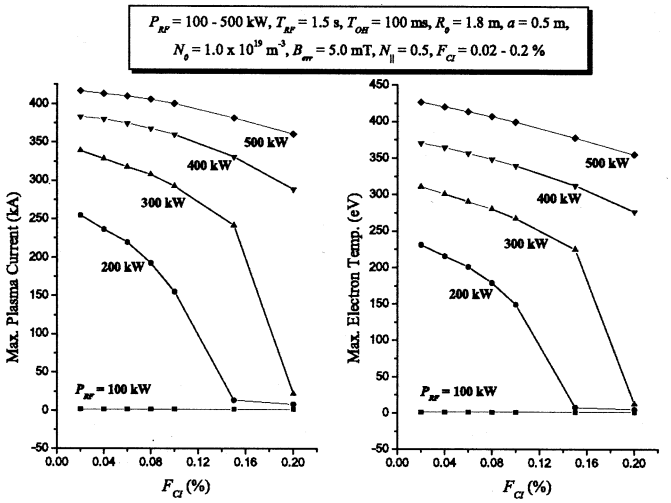

Fig. 9. Maximum plasma current and electron temperature as a function of the fraction of the carbon impurity (F_{CI}) to the electron density for RF powers of $P_{\mathrm{RF}} = 100$ kW–500 kW with a duration of 1.5 s.

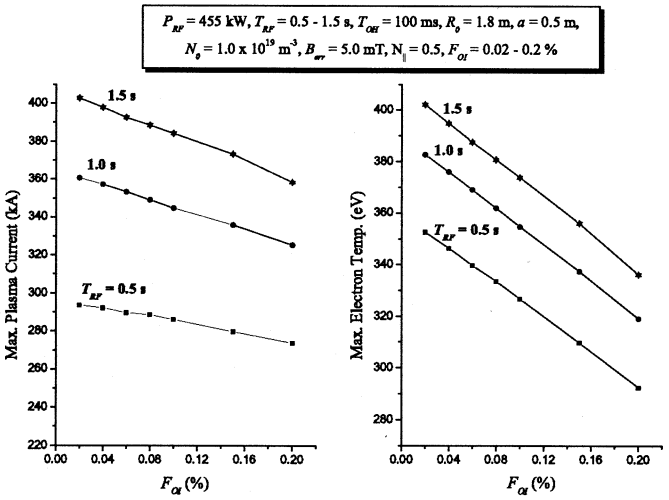

Fig. 10. Maximum plasma current and electron temperature as a function of the fraction of the oxygen impurity (F_{OI}) to the electron density for an RF power $P_{\mathrm{RF}} = 455$ kW with durations of 0.5, 1.0, and 1.5 s.

time $T_{\mathrm{OH}} = 100$ ms (1) for $P_{\mathrm{RF}} = 455$ kW with durations of 0.5, 1.0, 1.5 s; (2) and for $P_{\mathrm{RF}} = 100$ kW–500 kW with the duration of 1.5 s. The varied fractions of impurities to the electron density are as follows: the carbon $F_{\mathrm{CI}} = 0.02$–0.2%, the oxygen $F_{\mathrm{OI}} = 0.02$–0.2%, the iron $F_{\mathrm{II}} = 0.001$–0.006 95%. Figs. 8 through 13 show the maximum T_e and maximum I_p. The maximum plasma current and the maximum electron temperature do not decrease dramatically for the carbon and oxygen impurity densities up to 0.2% with an RF power of 455 kW. For the carbon and oxygen impurities up to 0.2% of the electron density, an RF power of 400 kW with a pulse length 1.5 s is adequate to give plasma startup. However, when the iron impurity is more than 6.5×10^{-3}% of the electron density, an RF power more than 455 kW need to be delivered with duration of 1.5 s. However, for the KSTAR ECH system, the RF power is limited to 455 kW because of the transmission loss.

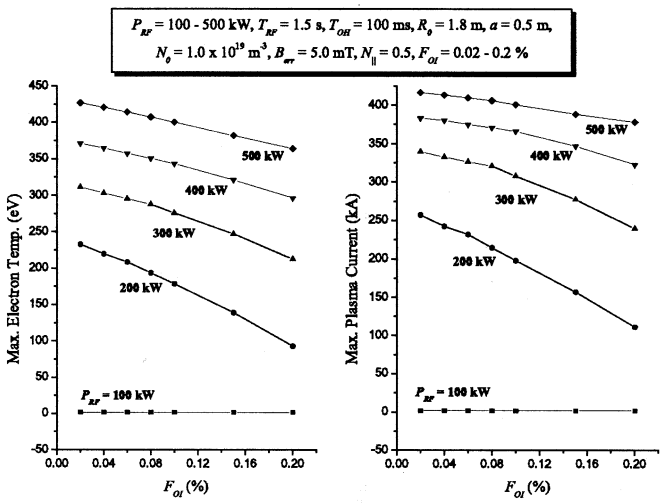

Fig. 11. Maximum plasma current and electron temperature as a function of the fraction of the oxygen impurity (F_{OI}) to the electron density for RF powers of $P_{\mathrm{RF}} = 100$ kW–500 kW with a duration of 1.5 s.

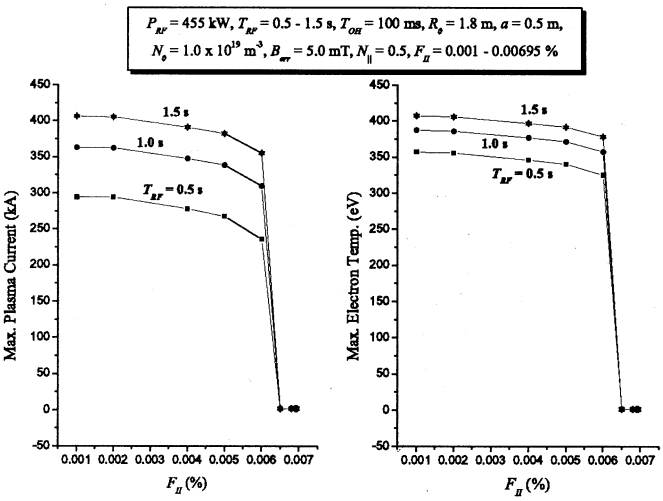

Fig. 12. Maximum plasma current and electron temperature as a function of the fraction of the iron impurity (F_{II}) to the electron density for an RF power $P_{\mathrm{RF}} = 455$ kW with durations of 0.5, 1.0, and 1.5 s.

IV. Conclusion

In the first phase KSTAR operation, the current scenario adopts the fast current ramping of seven pairs of poloidal field coils, and there will be no auxiliary heating except the ECH assist startup. In this paper, the preionization effects are investigated using 0-D code. As the RF pulse length and its power are increased, the dependence on the initial conditions, such as the ohmic heating delay time, the initial neutral density, the error field, and the impurity density is smaller for maximum electron temperature and plasma current. With the gyrotron RF power of 500 kW and 1.5 s, the preionization will minimize the dependence on KSTAR initial conditions except for very high impurity densities. In this work, we simplified the energy deposition and the plasma volume through the 0-D approximation. The many parameter scannings on the preionization effect are obtained easily using the 0-D code with small computing time. Further study will be attempted in a one-dimensional approximation.

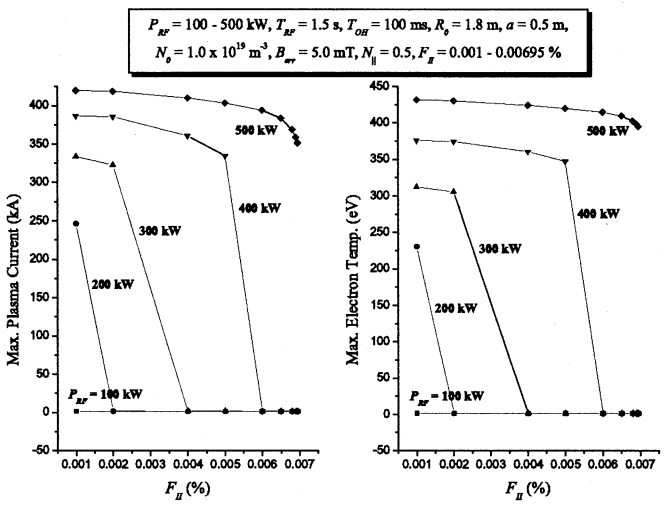

Fig. 13. Maximum plasma current and electron temperature as a function of the fraction of the iron impurity (F_{II}) to the electron density for RF powers of $P_{\mathrm{RF}} = 100$ kW–500 kW with a duration of 1.5 s.

Acknowledgment

The authors would like to thank Dr. O. Eldridge for his collaboration and his advice for the code.

References

[1] Y.-K. M. Peng, S. K. Borowski, and T. Kammash, "Microwave start-up of tokamak plasmas near electron cyclotron and upper hybrid resonances," *Nucl. Fusion*, vol. 18, no. 11, pp. 1489–1498, 1978.

[2] A. G. Kulchar, O. C. Eldridge, A. C. England, C. E. Bush, P. H. Edmonds, G. G. Kelley, C. M. Loring, Y.-K. M. Peng, J. B. Wilgen, and S. K. Borowski, "Preionization and start-up in the ISX-B tokamak using electron cyclotron heating at 28 GHz," *Phys. Fluids*, vol. 27, pp. 1869–1879, July 1984.

[3] V. V. Alikaev *et al.*, "Controlled fusion and plasma heating," in *Proc. 17th Eur. Conf.*, 1990, pp. 1080–1084.

[4] B. Lloyd, G. L. Jackson, T. S. Taylor, E. A. Lazarus, T. C. Luce, and R. Prater, "Low voltage ohmic and electron clyclotron heating assisted startup in DIII-D," *Nucl. Fusion*, vol. 31, no. 11, pp. 2031–2053, 1991.

[5] I. Fidone and G. Granata, "Electron cyclotron heating for assisted breakdown in next step tokamaks," *Nucl. Fusion*, vol. 34, no. 5, pp. 743–746, May 1994.

[6] C. Maroli and V. Petrillo, "Modeling of start-up assist by electron cyclotron waves for large-size tokamaks," *Il Nuovo Cimento*, vol. 10, pp. 677–691, June 1988.

[7] B. Lloyd, P. G. Carolan, and C. D. Warrick, "ECRH-assisted start-up in ITER," *Plasma Phys. Control. Fusion*, vol. 38, pp. 1627–1643, Sept. 1996.

[8] G. S. Lee *et al.*, "Design and construction of the KSTAR tokamak," *Nucl. Fusion*, vol. 41, pp. 1515–1523, Oct. 2001.

[9] A. C. England *et al.*, "Preionization modeling in KSTAR," *Bull. Kor. Phys. Soc.*, vol. 17, p. 427, 1999.

[10] Y. S. Bae, M. H. Cho, E. M. Choi, O. C. Eldridge, H. S. Kang, G. Y. Kim, K. H. Kim, I. S. Ko, and W. Namkung, "Impurity effects on preionization for KSTAR," in *Proc. 2000 Korea Accelerator and Plasma Research Association*, 2000, pp. 98–100.

[11] A. C. England, W. Namkung, O. C. Eldridge, M. H. Cho, I. S. Ko, G. N. Kim, H. S. Kang, and Y. S. Bae, "On preionization in KSTAR," *J. Accel. Plasma Res.*, vol. 5, no. 1, pp. 61–67, 2000.

[12] D. K. Lee, private communication, 2000.

[13] R. M. Gilgenbach *et al.*, "Electron cyclotron/upper hybrid resonant preionization in the ISX-B tokamak," *Nucl. Fusion*, vol. 21, pp. 319–327, 1981.

[14] O. C. Eldridge, W. Namkung, and A. C. England, "Electron cyclotron heating in tokamaks," Oak Ridge Nat. Lab., Oak Ridge, TN, Tech. Rep. ORNL/TM-6052, (W-7405-eng-26), Nov. 1977.
[15] P. G. Carolan and V. A. Piotrowicz, "The behavior of impurities out of coronal equilibrium," *Plasma Phys.*, vol. 25, no. 10, pp. 1065–1086, Oct. 1983.
[16] F. F. Chen, *Introduction to Plasma Physics and Controlled Fusion*, 2nd ed. New York: Plenum, 1984, vol. 1, p. 43.
[17] D. R. Cohn, R. R. Parker, and D. L. Jassby, "Characteristics of high-density tokamak ignition reactors," *Nucl. Fusion*, vol. 16, pp. 31–35, 1976.
[18] J. Y. Kim, private communication, 2000.
[19] *NRL Plasma Formulary*, 1998. revised.

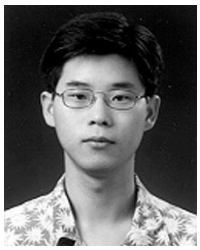

Young-soon Bae was born in Gangwon, Korea, on April 20, 1972. He received the B.S. degree from the Department of Physics, Chuang University, Seoul, Korea, in 1995 and the M.S. degree in physics from Pohang Univeristy of Science and Technology (POSTECH), Pohang, Korea, in 1998. He is currently working toward the Ph.D. degree at the Department of Physics, POSTECH.

In 1998, he spent one year as a Researcher in the Pohang Accelerator Laboratory. Currently, he is actively participating in the development of ECH and LHCD systems for KSTAR. His research interests include the basic plasma physics, the wave phenomena in high temperature magnetized plasma, accelerator beam physics, and particle simulation of low temperature plasma.

Mr. Bae is a member of the Korean Physical Society.

Won Namkung (M'83) was born on October 13, 1943, in Mokpo, Korea. He received the B.S. degree in physics from Seoul National University, Seoul, Korea in 1965 and the Ph.D. degree in physics from the University of Tennessee, Knoxville, in 1977.

He was a Research Associate and an Assistant Professor with the Electrical Engineering Department, University of Maryland, College Park, from 1978 to 1984. He was a Research Physicist with the Naval Surface Warfare Center, White Oak, MD, from 1984 to 1988. Since 1988, he has been a Professor with the Department of Physics and Pohang Accelerator Laboratory (PAL), Pohang University of Science and Technology (POSTECH), Pohang, Korea. His research interests include charged particle beams, fusion plasmas, EM wave-beam interactions, and particle accelerators. He was a leading member in construction of 2-GeV linear accelerator and the Director of PAL at POSTECH.

He is a member of the Korean Physical Society, the Korean Accelerator and Plasma Research Association, and the American Physical Society, and IEEE.

Moo Hyun Cho (M'95) received the B.S. and M.S. degrees from the Department of Nuclear Engineering of Seoul National University, Korea, and the Ph.D. degree in plasma sheath experiment from the University of Wisconsin-Madison in 1977, 1979, and 1988, respectively. He was a Post Doctoral Fellow from 1988 to 1989 at the University of Wisconsin-Madison.

Since 1989, he has been with the Department of Physics, Pohang University of Science and Technology, Kyungpook, South Korea, where he actively participated in the construction of 2-GeV electron linear accelerator, especially for the construction of the high power pulsed klystron system. His research interests include basic plasma physics experiment, high power microwave (Klystron), pulse-power technology, and their industrial applications.

Dr. Cho is a member of the Korean Physical Society, the Korean Accelerator and Plasma Research Association, the Korean Institute of Electrical Engineering, and the American Physical Society.

Alan C. England received the B.S. degree from the University of Illinois, Urbana, in 1954 and the Ph.D. degree from the University of Rochester, Rochester, NY, in 1961.

He was an Experimental Physicist with the Oak Ridge National Laboratory (ORNL), Oak Ridge, TN, from 1960 to 1995, where he worked in the Fusion Energy Division on the mirror machines PTF, ELMO, and INTEREM, as well as the tokamaks ORMAK, ISX-A, ISX-B, and finally the ATF Stellarator. He was a Visiting Scientist from ORNL at the Institute for Plasma Physics, Garching, Germany. He spent several years on assignment from ORNL at the Princeton Plasma Physics Laboratory (PPPL), Princeton, NJ, working on the tokamaks TFTR and PBX-M. In 1997 and 1998, was a Visiting Professor at the National Institute for Fusion Science, Tajimi, Japan, where he worked on the large helical device on electron cyclotron heating and ECE diagnostics. He worked for one year as a Visiting Scientist at the Pohang Accelerator Laboratory, Pohang University of Science and Technology, Pohang, Korea. He is currently a Visiting Scientist with the Device Development Division, Korea Basic Science Institute, Daejeon, Korea.

Dr. England is a member of the American Physical Society and the Korean Physical Society.